JOURNAL OF MATERIALS SCIENCE **39** (2004) 1943– 1958

Copper electrodes multilayer ceramic capacitors

Part I *The dielectric composition*

M. POLLET*, S. MARINEL
CRISMAT Laboratory, UMR 6508 CNRS/ISMRA, 6 B^d du M^al Juin-14050, CAEN, France
E-mail: michael.pollet@ismra.fr

Several sintering aids were tested to lower the $CaZrO_3$ ceramic sintering temperature. Numerous additions are shown to lower the densification temperature and to promote the dielectric properties with a QF product, an insulating resistivity and a permittivity enhancement, and a lowering of the temperature coefficient τ_ε. A combination of dopants was tested and optimised, resulting in a low temperature sintering ceramic based on $CaZrO_3$, $LiNO_3$, SiO_2 and TiO_2. The samples sintered at 1000°C in oxidising or reducing atmosphere exhibit very attractive properties, with a QF product of nearly 15, $\varepsilon \sim 28$, a near zero τ_ε and $\rho_i \sim 10^{12}\ \Omega \cdot$ cm. The sintering mechanisms of this ceramic are also debated.

1. Introduction

The aim of this study is to decrease the temperature of sintering of the $CaZrO_3$ material to allow a co-sintering with base metal electrodes and thus in the short term to produce base metal electrode-multilayer ceramic capacitors (BME-MLCC). The dielectric material chosen, $CaZrO_3$ has a relatively high permittivity (25–30), low losses and a high insulation resistivity.

This objective has two major constraints. The first is to have to sinter the material at temperatures lower than those of melting of the base metals (1083°C for copper and 1450°C for nickel). The second imposes to work under reducing atmosphere since these base metals oxidise very easily, losing thus their properties of good conductivity to become semiconductor. Initially, we were attached to the first point, the second one being only treated when a material with a sufficiently low sintering temperature was found.

The literature is very rich concerning the various ways of decreasing the sintering temperature. Many authors have noted a beneficial effect of the atmosphere control (nature of the atmosphere, pressure) during this stage. Readey & Ritland for instance have shown that an accurate checking of the atmosphere made it possible to control the porosity and the size of the pores [1]. Dominguez and Bigot have highlighted on nanometric iron powders that a reducing atmosphere could shift the temperature of the shrinkage rate's maximum to lower temperatures [2]. Conversely, Kutty *et al.* have evidenced on uranium oxides a lowering of 300–400 K of the temperature of the shrinkage rate's maximum while changing the atmosphere from a reducing to an oxidising one [3]. Harada has confirmed this result, observing a better densification and crystalline growth by increasing the partial pressure in oxygen [4]. Poirson *et al.* have noted a beneficial effect of the impoverishment in oxygen in the atmosphere for the sintering of the $La_{0.8}Sr_{0.2}MnO_3$ material [5]. This effect was attributed to an induced oxygen non-stoichiometry. More recently, we have observed that the $CaZrO_3$ material doped with manganese and tungsten could densify more easily, for an identical sintering temperature, using a reducing atmosphere [6, 7]. With regard to the present study, we have excluded this alternative to limit us to only two sintering atmospheres: first, the air, during a prospective step where we have exclusively attempted to decrease the sintering temperature; secondly, the final atmosphere used in the co-sintering process, a reducing atmosphere based on an argon/hydrogen mixture.

Another relatively effective means to decrease the temperature of sintering is to modify the grains size of the powder. Indeed, one can easily imagine that the lower the size of the particles is, the more the exchange surfaces are raised and thus the sintering is enhanced [8, 9]. Kanters *et al.* have modelled the compact's behaviour during the sintering while varying the initial particles size. They have shown, in the case where the mobility at the grain boundaries was the mechanism that dominates the growth, that higher densities could be reached if the initial particles were thinner [10]. Other simulations carried out by Darcovich *et al.* have highlighted that a broad grain size distribution could enhance the sintering [11]. According to their approach, the finest particles being absorbed by largest, the distribution is shifted to higher average sizes during the sintering and is broadened. As Shiau *et al.* have underlined, the disadvantage when increasing the grain size is to promote the grains growth and to facilitate the retention of intragranular pores, whereas a narrower distribution allows decreasing efficiently the grains

*Author to whom all correspondence should be addressed.

growth during the intermediate stage of the sintering to reach nearly 90% of the theoretical density [12]. In the particular case of a liquid phase sintering, Lumley and Schaffer have shown that flux particles of bigger sizes could be beneficial for the sintering if the solubility of the flux in the basic material was good enough [13]. Concerning the $CaZrO_3$ material, a study within the framework of a traditional treatment of the problem via a simple crushing has shown that this solution was efficient but unfortunately insufficient to decrease amply the sintering temperature, the grains size being not sufficiently reduced using this technique [6]. Nevertheless, note that a chemical way of preparation of this material has led Borglum and Buchanan to a similar conclusion concerning the beneficial effect of the reduction of the grains size [14].

As evoked above, the non-stoichiometry also promises an unnegligible opportunity to decrease the sintering temperature. By decreasing for instance the oxygen partial pressure in the atmosphere, vacancies can be created in the anion sub-lattice what can increase the mobility of the species in this sub-lattice; on the other hand, the reduced cations are bigger and their mobility are diminished; the stake is then to find the best compromise between these two antagonistic situations. In certain materials, it can also be interesting to modify the ratio between the different cations. Thus, for example, Kulcsar has observed that an excess of barium oxide in $BaTiO_3$ could reduce the crystalline growth, and that this low grains size contributed to reduce the sintering temperature [15]. Choi and Kim have confirmed this result in a more detailed study [16]. Haussonne *et al*., Desgardin *et al*. and later Tolino and Blum have shown that a ratio Ba/Ti > 1 was beneficial to the sintering of $BaTiO_3$ assisted by LiF or $BaLiF_3$, shifting the initial stage of the sintering to lower temperature, and increasing the shrinkage rate [17–19]. These two formers have attributed this effect to the formation of a solid solution of $BaTiO_3$ and $BaLiF_3$, which is partially responsible for the low sintering temperature. In the same way, Anderson and Proudian have highlighted in the $SrTiO_3$/LiF system that a ratio Sr/Ti > 1 was beneficial for the sintering [20] what has been corroborated by Haussonne *et al*. [21]. In this case, the non-stoichiometry promotes for the formers the liquid phase quantity whereas for the seconds, a mechanism similar to the case of $BaTiO_3$ is considered. More recently, on the contrary, Kleveland *et al*. have observed the effect of the ratio La/Co on the shrinkage of the $LaCoO_3$ and have shown that an excess of either La_2O_3 or CoO could increase the sintering temperature [22]. They have correlated this phenomenon to the higher melting point of the precursor as compared to the one of the final phase $LaCoO_3$. Lastly, related to $CaZrO_3$, a recent study has highlighted that a non-stoichiometry in zirconium or in calcium could shift the temperature of the maximum shrinkage rate to lower temperature with an optimum value close to 1% deficit of zirconium. Nevertheless, the most spectacular result is obtained by introducing the non-stoichiometry *a posteriori* by adding an excess of $CaCO_3$ to the stoichiometric phase. In this way, it has been shown that an addition of 5 mol% could shift the temperature of the maximum shrinkage rate to some 350 K [6].

Nevertheless, the most intensively used and most effective means to decrease the sintering temperature is the use of doping agents and/or additions. Thus, lithium salts have proved their effectiveness to lower the sintering temperature with materials such as $BaTiO_3$ [17, 19], $SrTiO_3$ [20, 21], $CaZrO_3$ [6] or AlN [23]. For the three formers, the shift in the sintering temperature is around 300–400 K while for the last, it reaches approximately 150 K. In the same way, the systems using the boron derivates are very numerous. For instance, the addition of B_2O_3 facilitates and accelerates the formation of the superconducting phase $Bi_2Sr_2Ca_2Cu_30_z$, without any degradation of the properties [24]. Kanai *et al*. have also noted a positive effect of B_2O_3 for sintering of lead-based perovskites, certainly due to the formation of an eutectic phase with a low melting point [25]. This same doping agent combined with ZnO is also very efficient to decrease the sintering temperature of $BaTi_4O_9$ shifting it from 1300 to 900°C [26]. Many other examples concerning the use of boron oxides are available in the literature [27–30]. Lastly, note that the use of BN additions has also been evidenced to be of great interest in the case of $(Ba_{0.92}Sr_{0.08})TiO_3$ ceramics, lowering the sintering temperature of nearly 100 K [31].

The majority of alkaline earth has also been tested in order to facilitate the shrinkage of ceramic materials. As already evoked, the calcium carbonate is an interesting sintering agent in the case of $CaZrO_3$ [6]. In the same way, strontium and barium oxide excesses have been shown to be beneficial in the cases of $BaTiO_3$ and $SrTiO_3$ [17–21]. The magnesium oxide is quite as attractive. Refer for instance to the studies of Haitao *et al*. who have shown its interest to densify Si_3N_4 [32] or those of Mori *et al*. with the $LaCrO_3$ material [33]. These later have moreover made an interesting comparison between the effects of magnesium, calcium and strontium oxides addition to their material: MgO offers the best advantages allowing for the same final density a sintering temperature 100 K lower than the others.

Many oxides with low melting points are also frequently used to decrease the sintering temperature of ceramics. Their list is interminable and the use of a specific one depends naturally on the system studied, then we will only on a purely illustrative basis mention some particular cases. Thus, the vanadium oxide V_2O_5 was used successfully by Huang *et al*. with $NdAlO_3$ ceramics, shifting the sintering temperature from 1650°C to nearly 1400°C, while maintaining the good dielectric properties of this material [34]. Its effect on the shrinkage is not always such satisfactory and in the case of $(Zr_{0.8}Sn_{0.2})TiO_4$, Huang *et al*. showed that the density decreased with the amount of V_2O_5 added [35]. Nevertheless, these authors have also shown that this system answered in a satisfactory way to copper or bismuth oxides additions reducing the sintering temperature from 1400 to 1300°C. Wang *et al*. have lowered the sintering temperature of the ferrite material $(Ni_{0.38}Cu_{0.12}Zn_{0.5})Fe_2O_4$ from 1250 to 1000°C by adding a mixture of glass made of PbO and SiO_2 or B_2O_3 mostly composed of PbO [36].

Rezlescu *et al*. have successfully lowered $Ni_{0.36}Zn_{0.64}Fe_2O_4$ ferrite powders sintering temperature using PbO [37]. MnO_2 is also an interesting particular case since it can also be used to protect the materials under reductive atmosphere [38–43]. It has been observed that manganese oxide could promote the densification of SnO-based ceramic [44] and SnO_2-based ceramic [45].

Lastly, and to finish with this non-exhaustive list, we can still evoke the derivatives of silicon which are abundantly used either as doping agents, or for their ease to form liquid phases with low melting points [46, 47].

Of course, all these various agents, though a number of them can be used alone, are very often combined to cumulate their various effects or to form new phases likely to enhance the sintering. We can mention for instance the $BaLiF_3$ phase, well-known in forming a solid solution with $BaTiO_3$ [18] or the numerous eutectic phases with low melting points such as those resulting from the PbO-WO3 system [48] or those resulting from the systems CaF_2-LiF, SrF_2-LiF, PbF_2-LiF [49–51].

The results reported in this paper are divided into two main parts: a first one describing the results obtained through a large prospective study implying the most frequently used sintering aids; the second one concerns exclusively the most efficient sintering aid found, which allows the sintering of $CaZrO_3$ bellow the copper melting point and moreover maintains the good properties of this dielectric material.

2. Experimental procedures

First, a stoichiometric $CaZrO_3$ phase was prepared using grade reagents (CERAC) $CaCO_3$ (99.95% purity) and ZrO_2 (99.95% purity). These two powders were wet-ball-milled in ethanol during 2 h in a Teflon recipient with zircon balls. The mixture was dried under infrared lamps and manually de-agglomerated in an agate mortar. This mixture was calcined in a tubular furnace (PIROX) at 1000°C during a 2 h dwell using a 150°/h heating/cooling rate.

All the additions were carried out using either carbonates, oxides or nitrates as will be specified in the results and discussion part. For the sintering aids used in the first part, the addition was systematically 5 mol%, the reference for one mole being $CaZrO_3$ and the percentage referring to the cation (for instance, the addition was 5 mol% for SiO_2 and 2.5 mol% for Bi_2O_3). The powders (i.e., the $CaZrO_3$ phase and the sintering aid) were wet-ball-milled in ethanol during 30 min. using an agate mortar with agate balls. The mixture was dried under infrared lamps and manually de-agglomerated in an agate mortar. An organic binder was added to the powder, which was then uniaxially pressed into green discs. 6.36 mm (diameter) discs for dilatometric measurements were pressed under a load of 2100 kg and 8.06 mm (diameter) discs for sintering were pressed under a load of 3880 kg.

In order to investigate the influence of these additions on the resulting phase, all of the synthesised powders and discs were analysed by X-Ray diffraction either with a Guinier's camera (ENRAF NONIUS FR590), with a SEIFERT diffractometer (Copper's K_{α_1} radiation) or a INEL X-ray generator equipped with a Huber four-circle goniometer and a position sensitive detector covering an angle of 120° (INEL CPS-120) with a spatial resolution of 0.03°.

Dilatometric measurements were carried out in static air using a SETARAM TMA92 dilatometer. For all the measurements, the temperature ramp was heated and cooled at 2°/min with a dwell at 1350°C for one hour. A slight charge of 1 g was applied to allow the measurements.

The co-fired sample was prepared using two 8.06 mmØ discs (around 1 mm thickness). One face of each was painted with a mix of copper powder and organic linker. The painted faces were placed facing each other and the two discs were pressed together under a charge of 3880 kg. Using base metal as inner electrode, the atmosphere of sintering was a 10%H_2/90% Ar mixture to avoid the metal reduction. The sintering temperature was 1000°C and a dwell duration of 6 hours was imposed. the heating rate was 2.5 K/min.

The polished samples were observed under a polarised optical microscope (Olympus BH2-HLSH) or, after gold-sputtering, using a scanning electron microscope (Philips XL30 FEG SEM).

Phase composition analysis was determined using an energy dispersive spectrometer coupled with the SEM (EDS—Oxford Link ISIS).

Electrical measurements were realized on shaped discs painted on both faces with an In-Ga eutectic paste and dried in an oven at 120°C. Insulating resistance measurements were obtained using a SEFELEC DM500A megohmmeter and the dielectric characteristics (ε, $tg(\delta)$) were acquired at 1 MHz with a FLUCKE 6306 LCR meter. The high frequency characteristics were measured through a cavity method.

3. Results and discussion

3.1. The effect of standard sintering aids addition

As already introduced, a large range of sintering aids has been tested. For this prospective phase, they were alternatively tested through dilatometric measurements, then they were sintered; their dielectric properties were measured and the samples were analysed using X-ray diffraction and observed using the SEM. All the tested sintering aids are shown in Fig. 1. The effect of lithium salts has already been published [6, 7] and will not be further discussed in this part. The alkali-earths have been retained for their efficiency as sintering aid [6, 17–21, 32, 33] as well as, dealing with the barium and strontium ions, for their ability to form a solid solution with $CaZrO_3$ and enhance the dielectric properties [52–54]; the magnesium oxide has been observed to not enter the $CaZrO_3$ structure [55]. The ions from the same column as the zirconium in the periodic table have been chosen for the same reasons. The ions from the same column as the vanadium in the periodic table have been tested for two reasons: a first evident one is the low melting point of the vanadium oxide (670–685°C [56]);

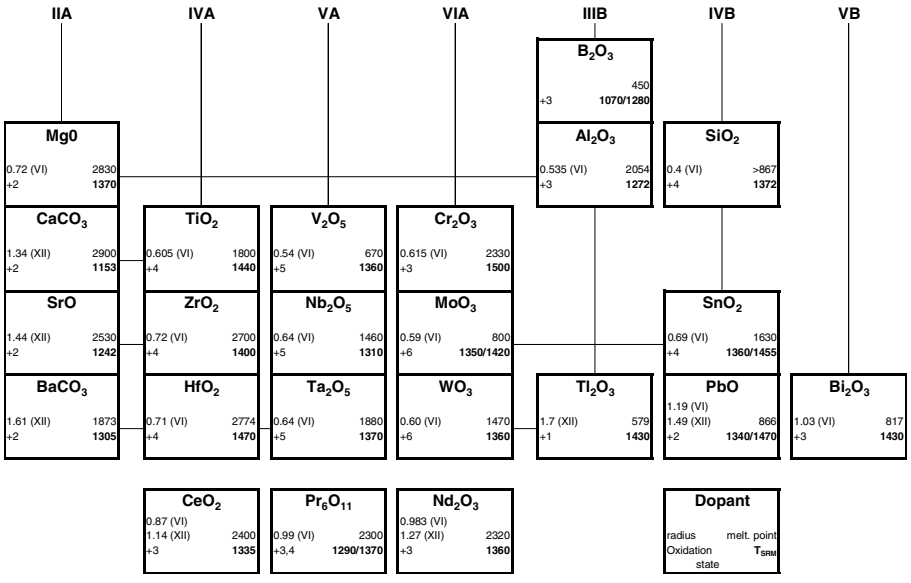

Figure 1 Tested allows to try to improve the sintering behaviour of $CaZrO_3$ ceramics; the legend is given in the lower-right box.

the second one is their small radius size in the six-fold coordination [56] which could facilitate their insertion in the $CaZrO_3$ structure and enhance the mobility in the cationic sub-lattice ($^{VI}Zr^{4+} = 0.72$ Å). A similar consideration was made for choosing the chromium oxide and the cations of the same column, since MoO_3 melts at nearly 800°C and the ion radius in the six-fold coordination are 0.615, 0.41, 0.42 for respectively Cr, Mo and W [56]. The boron oxide was evidently tested because of its low melting point (450°C [56]). The aluminium oxide was chosen for two reasons: the first one is due to an experimental observation, which has shown that our material was reacting with the Al_2O_3 made-of recipient, through the formation of a liquid-like phase; the second one is that the radius of the aluminium cation is 0.535 in the six-fold coordination [56] which can promote its mobility in the cationic sub-lattice. The thallium, lead and bismuth oxides were chosen for their ability to melt at low temperature: respectively 579, 866 and 817°C for Tl_2O, PbO and Bi_2O_3 [56]. Tin oxide has a high melting point (1625°C [56]) and Sn an ionic radius in the same order as the Zr one (0.69 Å), nevertheless, it has been shown that the $BaTi_4O_9$ ceramic sintering temperature could be lowered using this agent [57]. SiO_2 has been chosen for the low melting point of its amorphous phase. Finally, a few rare earths were also studied: Badenes *et al*. have observed that a praseodymium doping was beneficial since Pr could enter the CaO-ZrO solid solution and could improve the ceramic densification [58]. Arbitrarily, it was decided to observe the behaviour of the praseodymium neighbouring ions in the periodic table, i.e., cerium and neodymium. The resulting behaviour depends of course of the doping agent. Classically, the observations follow this scheme: (i) if the addition is able to melt, the densification can be enhanced by a liquid phase sintering; (ii) if the added specie reacts with the base-material, it can lead either to the formation of a liquid phase and this case is the same as the upper-mentioned one, (iii) or the new phase can eventually promote the diffusion; (iv) the addition can simply enhance the diffusion; (v) finally, nothing can happen. Note that for convenience, all the tested additions will be referred with the name of the cation in the following (for instance, Ba addition for BaCO3 addition, Pr addition for Pr_6O_{11} addition, . . .).

The dilatometric measurements for the alkali earths are shown in Fig. 2. Only the densification rate (calculated from the shrinkage data assuming an isotropic densification) is plotted, since it offers a better mean to compare the results (the temperatures written near the curves are the one for which the shrinkage is almost finished). The result for a $CaCO_3$ addition (5 mol%) from reference 6 is also given for comparison. Except for MgO (which does not present any twelve-fold coordination) it is evidenced that the smaller the ionic radius is (respectively 1.34, 1.44, 1.61 Å for Ca, Sr, Ba in the twelve-fold coordination [56]), the lower the temperature to achieve the shrinkage rate maximum (SRM) is. In the same way, the SRM decreases with the ionic radius. Concerning the sintering temperature (T_S), i.e., the temperature that coincides with the almost ended shrinkage, it is noticeable that these three additions allow its decrease. The case of $CaCO_3$ addition, which is the most favourable, has already been debated [6]. Since no liquid phase formation is expected for such low temperatures, these behaviours may be interpreted as a diffusion enhancement. It could arise from the formation of a solid solution $(CaX_y)ZrO_{3+y}$ ($X = $ Ca, Sr or Ba) as suggested in [6]. In such a solid solution, the induced vacancies should enhance the mobility in both the cationic and anionic sub-lattice. As evoked just above, the behaviour with an Mg addition follows a different trend. All the parameters (SRM, T_{SRM}, T_S) are improved but the changes are very slight. As already said, the Mg ion is not able to adopt a twelve-fold coordination (except using hard conditions, as it is the case for the perovskite $MgSiO_3$ in the earth mantle [59]). Nevertheless, it is well known that it can easily enter six-fold sites as it is the case in the mixed perovskites $Ba(Mg_{1/3}Ta_{2/3})O_3$ [60, 61], $Ba(Mg_{1/3}Nb_{2/3})O_3$ [61] and $Sr(Mg_{1/3}Ta_{2/3})O_3$ [62], or in the illmenite $MgTiO_3$ [63]. Its six-fold coordination ionic radius is 0.72 Å,

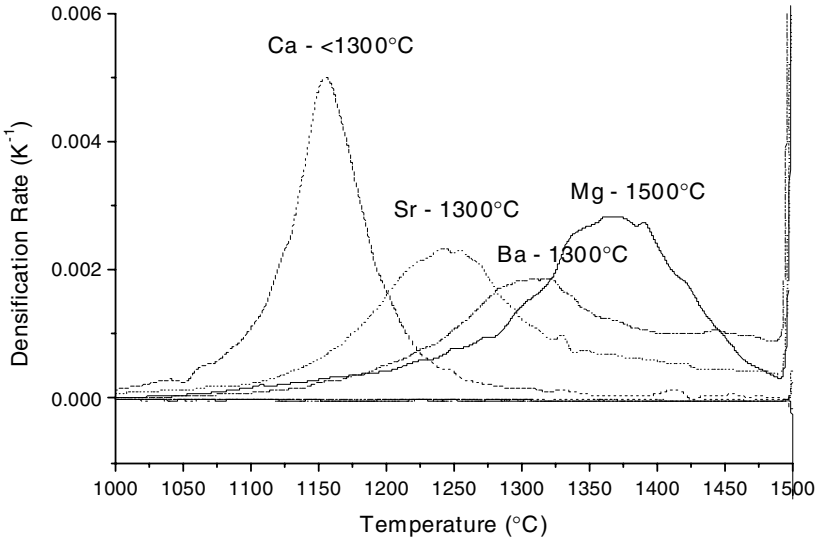

Figure 2 Densification rates in the case of a doping with MgO, $CaCO_3$ [6], SrO_2 and $BaCO_3$ (The estimated ending shrinkage temperature is written near the alloy).

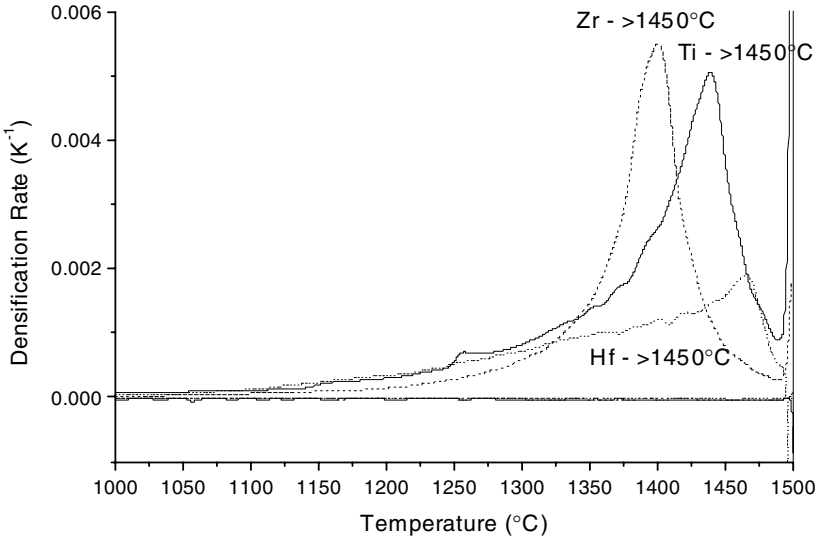

Figure 3 Densification rates curves in the case of a doping with TiO_2, ZrO_2, and HfO_2 (The estimated ending shrinkage temperature is written near the alloy).

which is the same that the zirconium one in this neighbourhood. This could explain why its behaviour is so far from those of the other alkali earths. Anyway, as can be seen in Fig. 3, its behaviour is more similar to the one of the zirconium [6] and co-allows. Except for the Hf doping, the dilatometric results show that T_{SRM} is slightly decreased for all these doping (Zr, Ti and Mg) with the best result obtained, concerning the atoms of the zirconium column in the periodic table, with the zirconium oxide (T_{SRM} ~1400°C); Mg doping leads to a better improvement with T_{SRM} ~1370°C. It can also be noted that the SRM is maximum with a Zr doping, slightly decreases with the Ti doping and is vanishing with the Hf doping resulting in a behaviour almost similar to the one of the pure $CaZrO_3$ material. In all theses cases, T_S is upper than 1450°C. This behaviour of slight improvement in the case of a B site doping (in the perovskite ABO_3) suggests a low mobility of the species in this site, which is a well-known purpose in these structures. The fact that the T_{SRM} with an Mg doping is somewhat better may be due to the lattice defects induced in the anionic sub-lattice, since its entering in the lattice should imply the release of an oxygen ion (ZrO_2/MgO_1), allowing an extended mobility in the anionic sub-lattice. This reduction is also to some extent to decrease the strain in the lattice and could also allow a diminution of the activation energy for the diffusion of the Mg doping. Note that another interpretation very close to the previous one is simply to consider the formation of a non-stoichiometric phase where the A site of the perovskite and the anionic site would be deficient. In the case, the diffusion through these deficient sites would be obviously increased. The fact that the improvement is weak could result from a very sharp domain for the solid solution as evoked in [6]. The densification rates for the vanadium, niobium and tantalum oxides doping are plotted in Fig. 4. The most surprising effect is the one obtained using the vanadium oxide; it was chosen for its low melting point that could make the sintering begins at lower temperature.

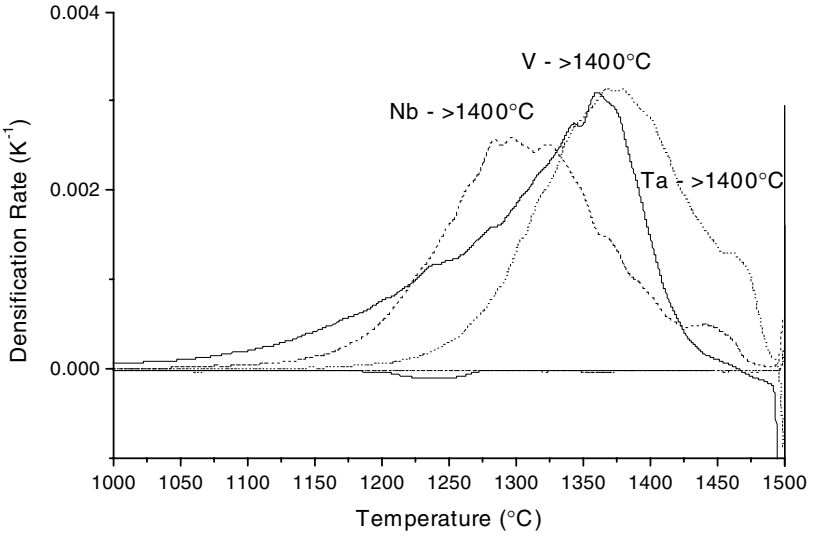

Figure 4 Densification rates curves in the case of a doping with V_2O_5, Nb_2O_5, and Ta_2O_5 (The estimated ending shrinkage temperature is written near the alloy).

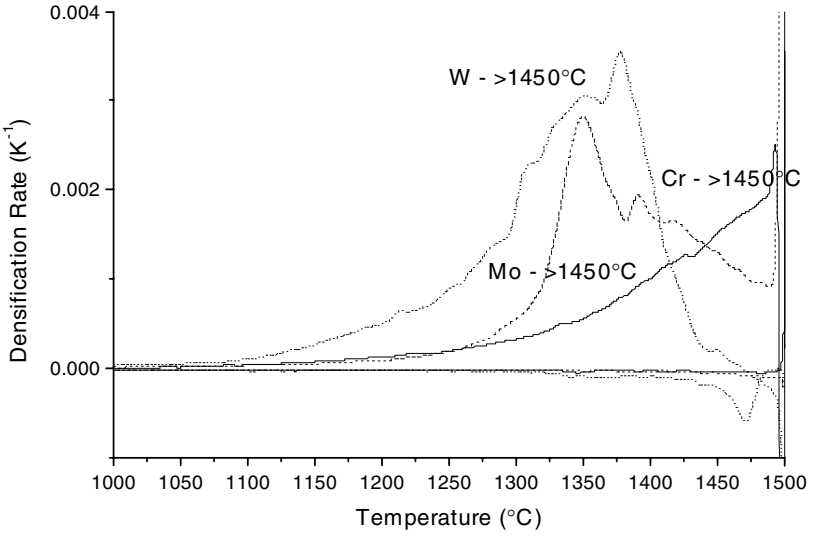

Figure 5 Densification rates curves in the case of a doping with Cr_2O_3, MoO_3, and WO_3 (The estimated ending shrinkage temperature is written near the alloy).

Here, it hardly begins at around 800°C, which seems to show that there were no or few liquid phase, is maximum at 1360°C and ends at roughly 1450°C. T_{SRM} for Nb and Ta are respectively 1300 and 1400°C, T_S being higher than 1450°C. These three additions present a SRM higher than the one of the $CaZrO_3$ material ($\sim\times 3$). As in the case of the zirconium, the improvement is very slight, nevertheless, for these three doping, the sintering starts earlier. The interpretation could be as in the previous case that the entrance of these atoms in the B site of the perovskite induces a non-stoichiometry in the A site and to a lower extent in oxygen, enhancing the diffusion through both the A site diffusion path and the anionic sub-lattice: $CaZrO_3 + 2.5\%X_2O_5 \rightarrow Ca(ZrX_{0.05})O_{3.125} = Ca_{0.952}(Zr_{0.952}X_{0.048})O_{2.976}$. The main difference between the previous case and this one stands in the valence of the doping element: +4 for Ti, Zr, Hf and +5 for V, Nb and Ta. Following the scheme of the deficient A site and anionic sub-lattice, it results in a less deficient anionic sub-lattice in the second case. Nevertheless, no evidence for this purpose has been found. The densification rates for the chromium, molybdenum and tungsten oxides doping are presented in Fig. 5. Here again, no meting is clearly evidenced, although MoO_3 melts at 800°C. These three dopants allow a sintering beginning at around 900°C and the densification continues up to temperature higher than 1450°C, the worst case being with the chromium doping for which the end of the shrinkage is not visible through this experiment. Note that this last ion is the one having the highest radius in the six-fold coordination (the lowest radius being for the Mo ion), which could partially explain the poor results obtained. Note moreover than considering the entrance of the dopant in the $CaZrO_3$ structure, this would lead to $Ca_{0.952}(Zr_{0.952}X_{0.048})O_3$, that is to say a non-deficient anionic sub-lattice. This last point could explain the very slight (W, Mo) or non-existent (Cr) improvement of the sintering behaviour. The densification rates for the materials with a B_2O_3, SiO_2 or Al_2O_3 doping are shown in Fig. 6. The SiO_2 contribution to the enhancement of the densification is very slight and

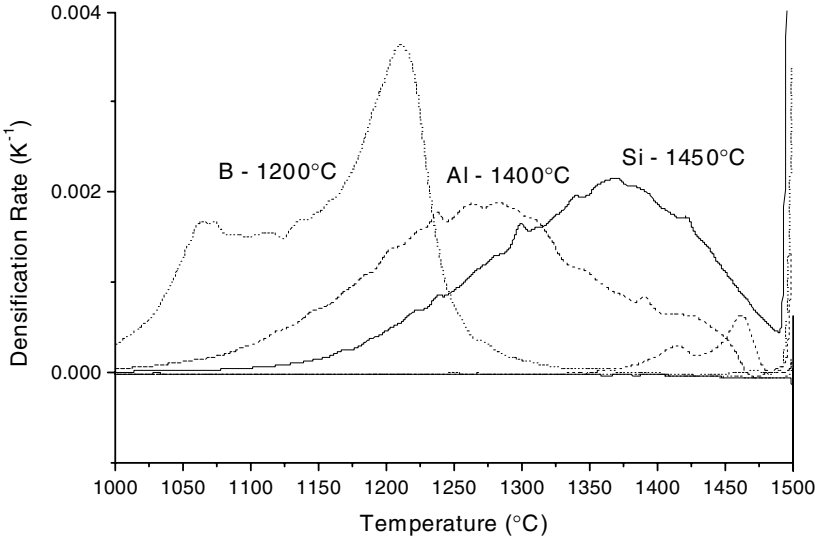

Figure 6 Densification rates curves in the case of a doping with Al_2O_3, SiO_2, and B_2O_3 (The estimated ending shrinkage temperature is written near the alloy).

the shrinkage is almost ended at 1500°C. With Al_2O_3 doping, $T_{SRM} = 1270$°C and $T_S \sim 1400$°C. In both cases, the SRM is barely twice the one of $CaZrO_3$. The behaviour of the Al_2O_3-doped material might be related to the formation of the liquid-like phase already evoked. No phase diagram between $CaZrO_3$ and Al_2O_3 has been found that could account for the formation of this liquid phase. Fischer *et al*. have established that the eutectic temperature is 1910 ± 20°C [64], which is obviously too high to account for our observation. Nevertheless, Chaterjee *et al*. have reported a eutectic temperature in the CaO-Al_2O_3 system of about 1390°C [65]. This temperature, although too high to explain the SRM could be correlated to the incident observed on the densification rate curve. The result obtained with B_2O_3 is the most interesting, with $T_S \sim 1200$°C. It exhibits a two steps behaviour with $T_{SRM1} \sim 1070$°C and $T_{SRM2} \sim 1280$°C. The results for the thallium, lead and bismuth oxides are presented in Fig. 7. On this figure is although plotted the result for SnO_2. Although the three formers have low melting points, no evidence for a liquid phase sintering can be deduced from the curves. None of these three aids display any positive (nor negative) effect and will not further be discussed. The SnO_2-doped material exhibits a three steps behaviour with $T_{SRM1} = 1360$°C, $T_{SRM2} = 1400$°C and $T_{SRM3} = 1455$°C. It can also be noted that a dilatation is also observed on the densification rate curve and centred at around 1260°C. We were not able at this stage to find any explanation for these behaviours. Finally, the last case tested is the doping with rare earths. Their densification rate curves are plotted on Fig. 8. These dopants are supposed to enter either the A site or the B site of the perovskite (or both) structure since they can have either a six- [66, 67] or twelve-fold coordination [67]. Their T_{SRM} are 1325°C for CeO_2, 1280 and 1380°C for Pr_6O_{11} that exhibits a two steps behaviour, and finally, 1350°C for Nd_2O_3. All these materials have a $T_S > 1450$°C and no obvious particular trend seems to be evidenced from this analysis.

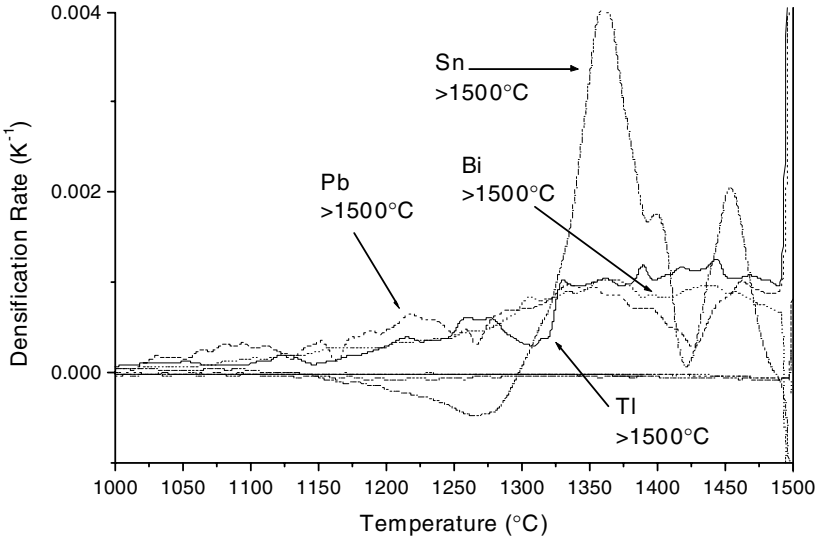

Figure 7 Densification rates curves in the case of a doping with Tl_2O_3, PbO, Bi_2O_3 and SnO_2 (The estimated ending shrinkage temperature is written near the alloy).

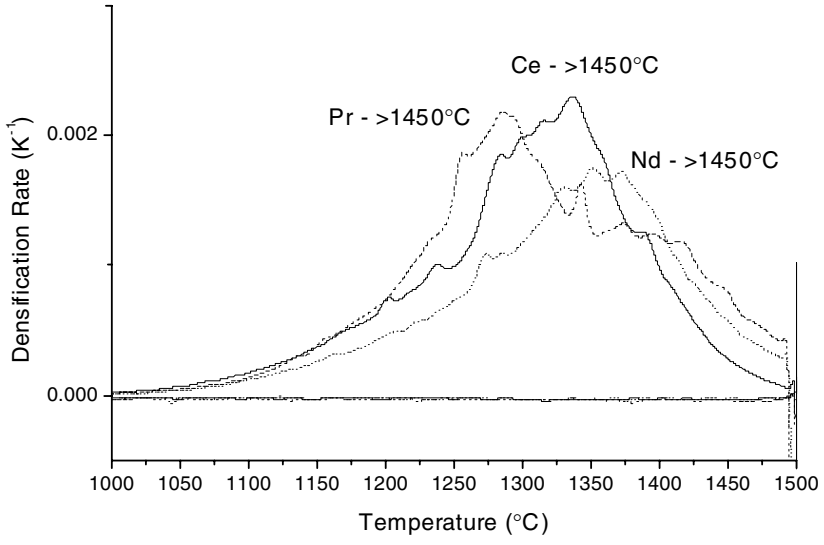

Figure 8 Densification rates curves in the case of a doping with CeO_2, Pr_6O_{11} and Nd_2O_3 (The estimated ending shrinkage temperature is written near the alloy).

Finally, this first prospective stage can be summarised in this way: (i) none of the addition normally able to melt at low temperature has formed any apparent liquid phase; (ii) the most efficient additions are the twelve fold coordinated alkali earths and B_2O_3; (iii) the firing temperature seems highly dependent on the oxidation state of the B site ion, the SRM being generally reduced with its increase (see columns IVA, VA and VIA in Fig. 1; the stable oxidation state of the chromium ion is +3).

Although these additions did not allow sufficiently reducing the sintering temperature, all the doped-materials were sintered in order to characterise their dielectric properties. They were fired at 1400°C during 12 h except the B_2O_3-doped sample that was fired at 1200°C. The final relative density and the properties are summarised in Fig. 9. Note that not all the QF values could be measured due to the bad shapes of several samples inadapted to the measurement by the cavity method. Unsurprisingly, the less densified samples correspond to ones that have the highest T_{SRM}. Nevertheless, the minimum density obtained is nearly 85% of the theoretical one for the Cr_2O_3-doped material. A representative microstructure of the alkili earths-doped samples is in Fig. 10 except for the MgO-doped as illustrated in Fig. 11. For the three formers (Ca, Sr and Ba-doped materials) the grain size is comprised between 0.5 and 2 μm, whereas the Mg-doped sample exhibits a great coarsening of the grains that reach sizes greater than 40 μm. The samples doped with alloys containing element of the zirconium column are well represented by the microstructure presented in Fig. 12 with grains sizes comprised between 1 and 3 μm. These seven samples did not show any secondary phase neither using X-ray diffraction, nor EDS. Besides, the EDS results account for an homogeneous repartition of the

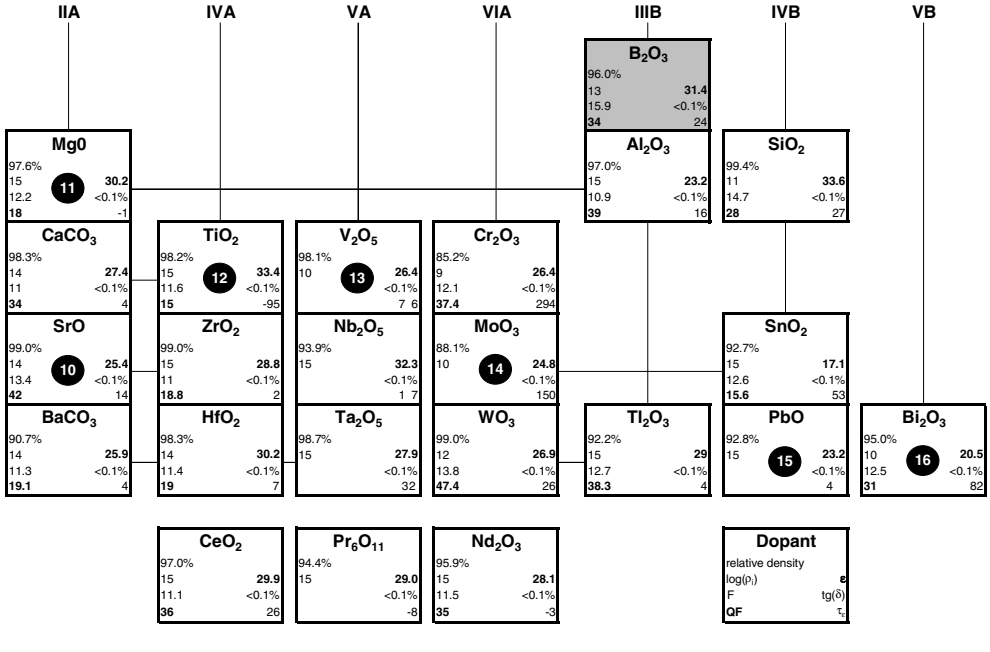

Figure 9 Relative density and dielectric results; the legend is given in the lower-right box (The grey box indicates a sintering at 1200°C).

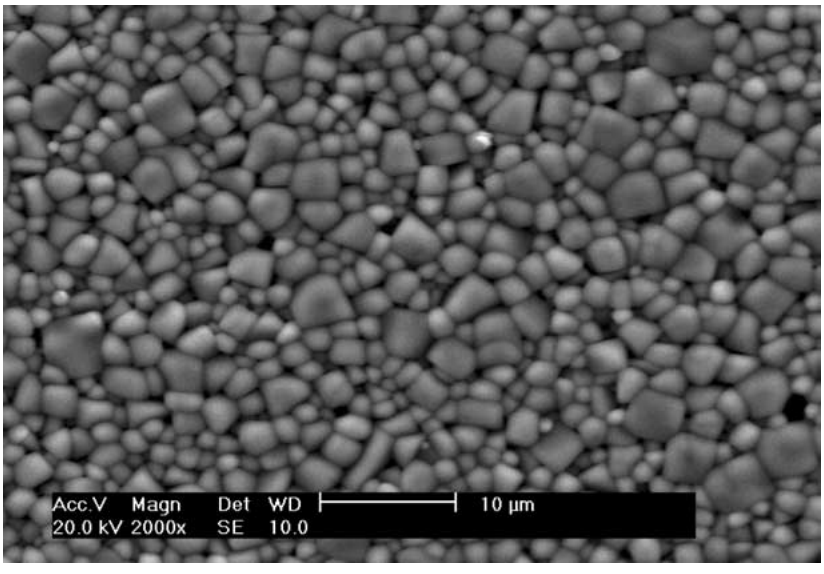

Figure 10 Representative microstructure of an alkali earth-doped sample.

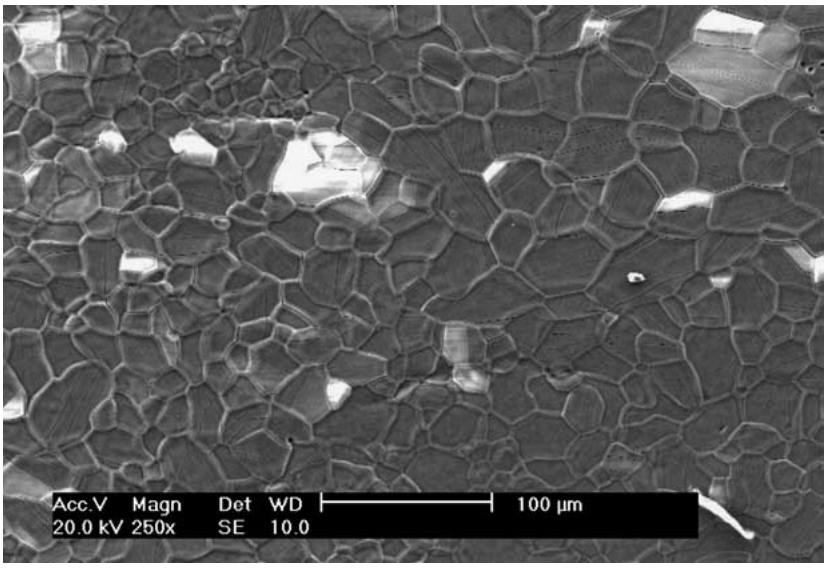

Figure 11 Microstructure of an MgO-doped sample.

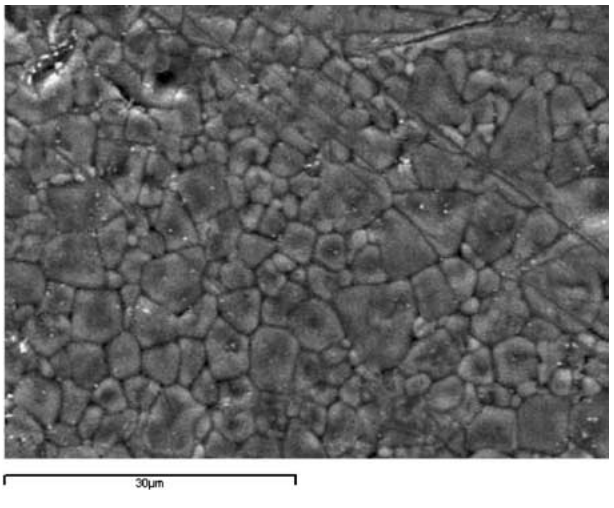

Figure 12 Microstructure of a TiO_2-doped sample.

doping elements in the material and for the entrance of the alkali earths in the A site of the perovskite and of the Ti, Zr and Hf ions in the B site. In the same way, the repartition of Nb and Ta seems to be homogeneous and no secondary phase was here again observable. On the other hand, the vanadium oxide has a different behaviour with the formation at the interface of the grains of a phase apparently composed of $CaVO_3$ [68] identified using the EDS (Fig. 13); nevertheless, such a phase could not be detected through X-ray diffraction. It is also noticeable that ZrO_2 particles are observable. An interpretation could be that the zirconium could have a poor miscibility in the vanadium oxide liquid or that the calcium could have a great one; thus on the vanadium oxide melting, the ion the most able to diffuse in the flux should be the calcium that leaves the $CaZrO_3$ matrix; on cooling, there should remain $CaZrO_3$, ZrO_2 because of the departure of the calcium and $CaVO_3$ because of the affinity of Ca with the vanadium oxide. Since the mobility of one of the ions should be reduced and the other one enhanced, the behaviour during the sintering should be mixed: on one hand the temperature of the beginning of the sintering should be lower than the one expected for $CaZrO_3$; on the other hand, the end of sintering should be merely constant or slightly shifted depending on the advance in the densification.

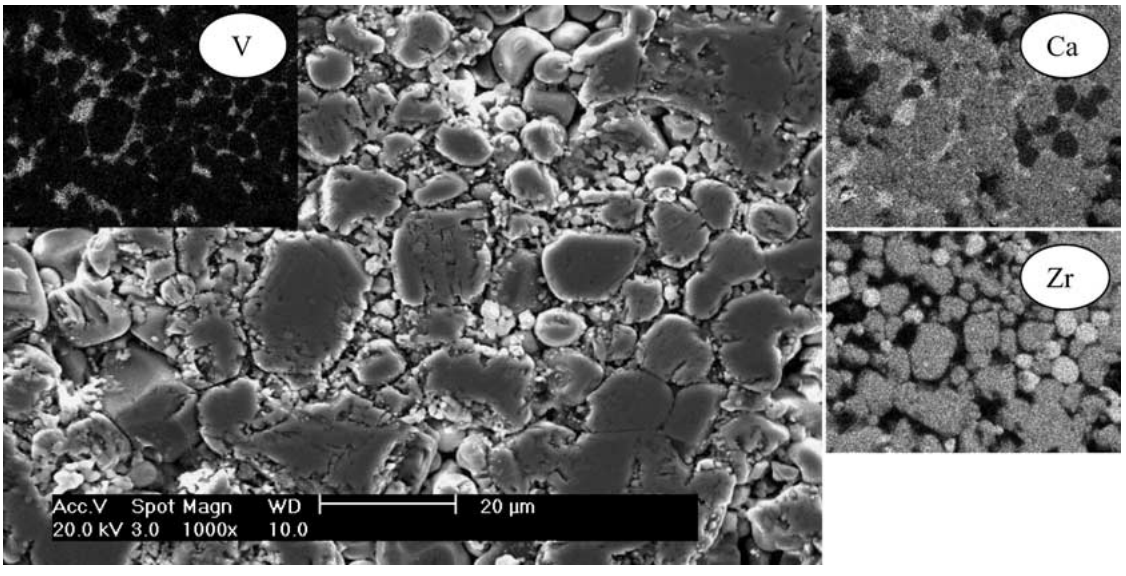

Figure 13 Microstructure of a V_2O_5-doped sample. The insets are the cartographic EDS analysis.

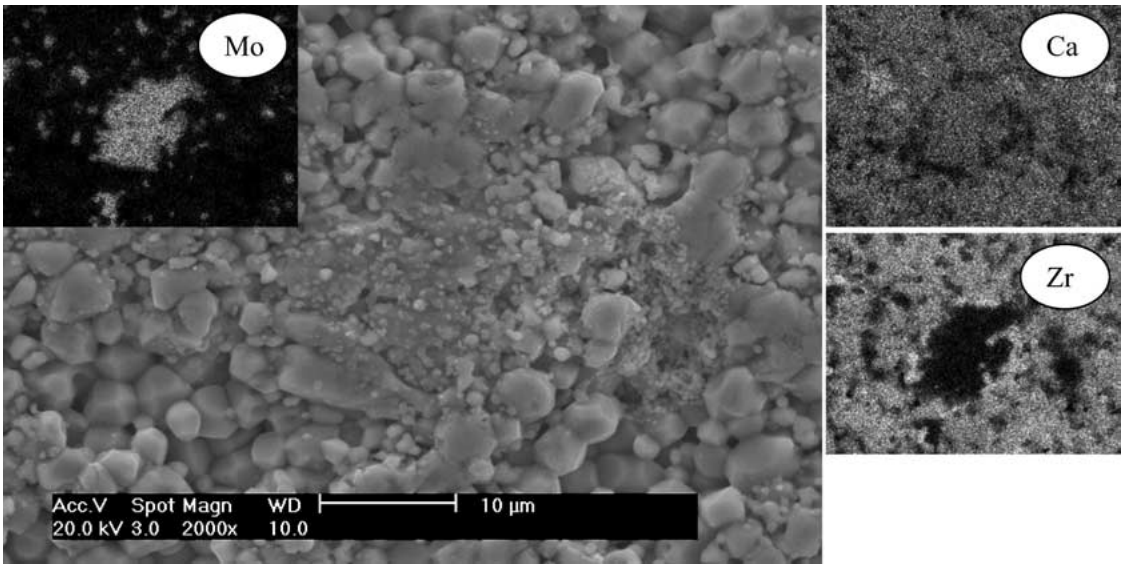

Figure 14 Microstructure of a MoO_3-doped sample. The insets are the cartographic EDS analysis.

This interpretation seems to be roughly in agreement with the result plotted in Fig. 4, with a shrinkage beginning slowly at around 800°C ($T_m[V_2O_5] = 670$°C), a soft slope in rate up to the SRM and a end of the densification at around 1450°C. Of course, further experiments are necessary to confirm or invalidate this interpretation. The microstructure accounts for a similar behaviour with MoO_3 (Fig. 14). The secondary phase has a composition compatible with $CaMoO_4$ [69] although X-ray diffraction could not evidence its formation. Contrary to the case of V_2O_5-doped material, this phase is not homogeneously distributed and is grouped in heaps in the material. No other phase than $CaZrO_3$ and the assumed $CaMoO_4$ has been evidenced. The $CaZrO_3$ particles size is around 2 μm. If the densification rate curve plotted in Fig. 5 is examined again, an interpretation almost similar to the one exposed for V_2O_5 can be submitted. The W- and Cr-doped materials present the same microstructure with fine grains (≤ 1 μm) and a good apparent density, confirmed the measured ones. A secondary phase is detected in the case of the W-doped material; this phase observed only using the EDS is compatible with the $CaWO_4$ composition [69]. Nevertheless, this phase is extremely in the minority. Concerning the rare earths doping, the samples containing either praseodymium or neodymium display a homogeneous composition and the EDS results show that the doping ion enters the A site of the perovskite. The behaviour with the cerium oxide is somewhat different with the formation of a secondary phase of composition determined through EDS as $Ca_{0.13}Zr_{0.27}Ce_{0.6}O_z$. This phase could not be detected through X-ray diffraction. Nevertheless, such a phase exists in the CaO-ZrO_2 system with the composition $Ca_{0.134}Zr_{0.866}0_{1.866}$ [70], which is in very good agreement with the upper found composition if it is admitted that the cerium ion replaces a part of the zirconium. Of course, as already evoked, such a hypothesis could not be validated since this phase does not appear on the X-ray patterns. Concerning the lead and neighbouring ions doping, the results are dispersed. The thallium oxide seems to not or fewly participate to the sintering since the particles of

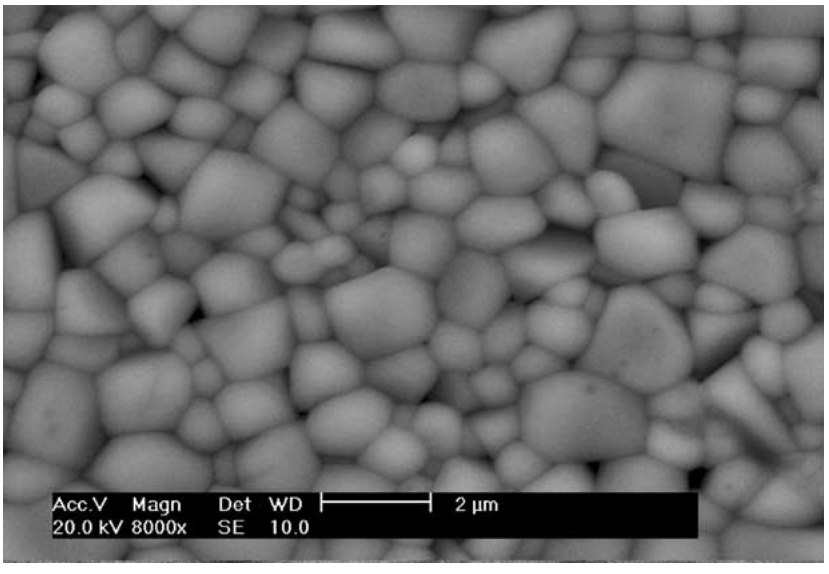

Figure 15 Microstructure of a SnO_2-doped sample.

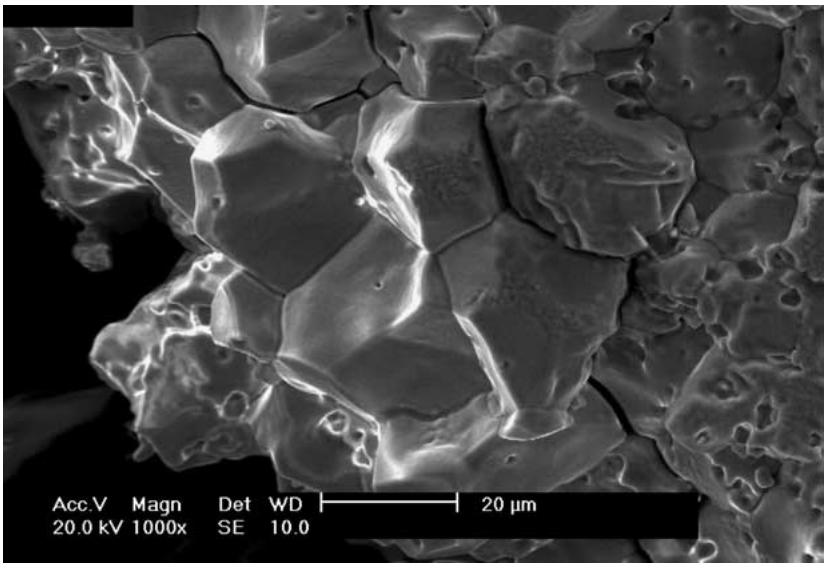

Figure 16 Microstructure of a Bi_2O_3-doped sample.

Tl_2O_3 are clearly observable using the SEM and that no other traces of Tl can be found in the sample, neither in the $CaZrO_3$ grains nor at the grain boundaries. Using the tin or lead oxides, the result is quite similar (Fig. 15) with well-densified ceramics; the grain size is respectively 3–5 μm and 0.75–2 μm. Using the bismuth oxide, the ceramic is also well-densified and the grains have grown to reach nearly 20 μm (Fig. 16). In these four cases, the dopant seems to be homogeneously distributed in the ceramic. Using SiO_2, the material contains 2 phases: $CaZrO_3$ in the majority and $CaSiO_3$ distributed homogeneously in the ceramic. The use of Al_2O_3 makes the material become biphasic (Fig. 17), with smaller grains composed of $CaZr_4O_9$ [71] and larger ones composed of $CaZrO_3$. The repartition of the minority phase ($CaZr_4O_9$) is not homogeneous and concentrates in the bulk of the sample. The results with B_2O_3 were encouraging since it was sintered at 1200°C and displayed a high density. Unwisely, additional tests have shown that increasing the amount of

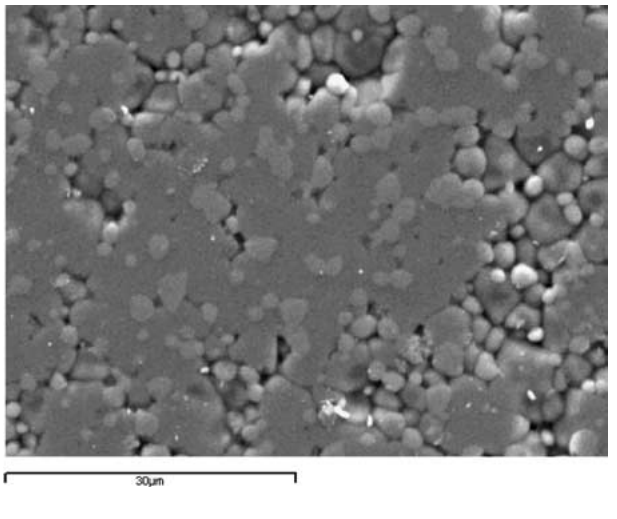

Figure 17 Microstructure of a Al_2O_3-doped sample.

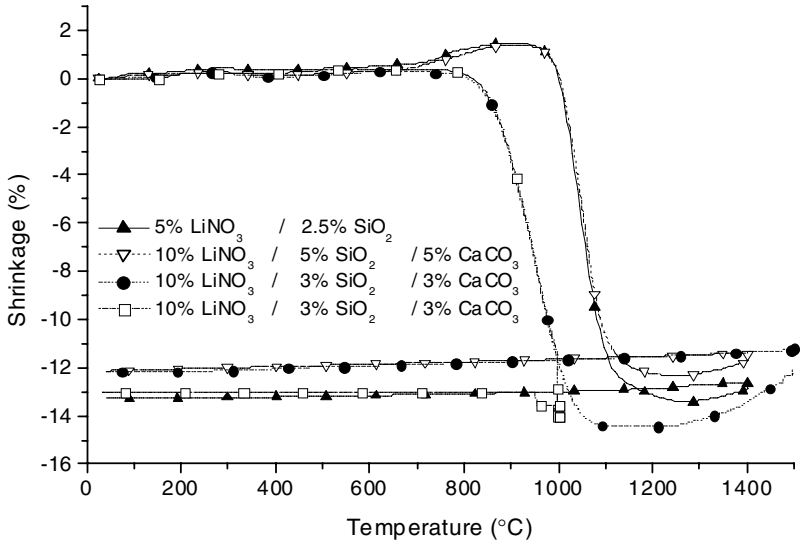

Figure 18 Dilatometric measurements of $LiNO_3$-SiO_2-$CaCO_3$-doped $CaZrO_3$ materials.

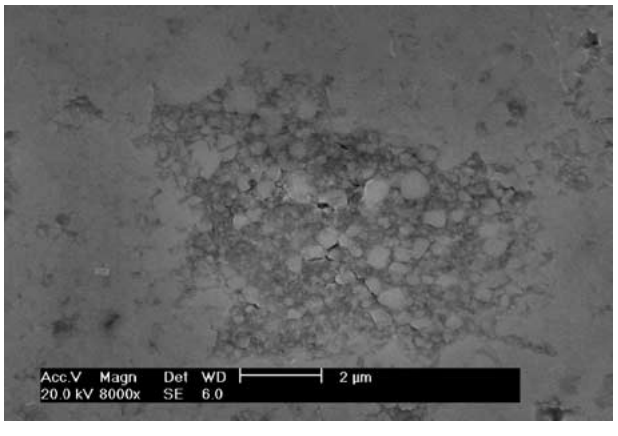

Figure 19 Microstructure of a CZ-LSC sample.

B_2O_3 was not efficient to reduce significantly more the sintering temperature.

The permittivity at round temperature for all the tested compositions has an average value of 27.5, the larger decrease being with the SnO_2 and Bi_2O_3 doping (17.1 and 20.5) and the larger increase with SiO_2 and TiO_2 (33.6 and 33.4). Unfortunately, no particular trend can be evidenced from these measurements concerning the effect of the different dopants. All the temperature coefficients (τ_ε) are less than 100 ppm/K except those of the Cr_2O_3 and MoO_3 doped materials. Note that only four are found negatives: -1, -95, -8 and -3 for respectively the MgO, TiO_2, Pr_6O_{11} and Nd_2O_3 doped materials. The insulating resistivities are generally more than 10^{14} Ω·cm except with additions of bismuth, silicon, vanadium and the elements in column VIA in the periodic table (the values reported with $\rho_i \leq 10^{10}$ Ω·cm have a poor accuracy). All the high frequency Q factors were measured at round temperature and among all the tested samples, the WO_3 and SrO-doped samples display the most important QF product with respectively 47.4 and 42 THz; nevertheless, numerous other elements allow values greater than 30 THz (Ca, Cr, Ce, Nd, Al, Tl, Bi). It would have been of great interest, in order to still improve this value, to

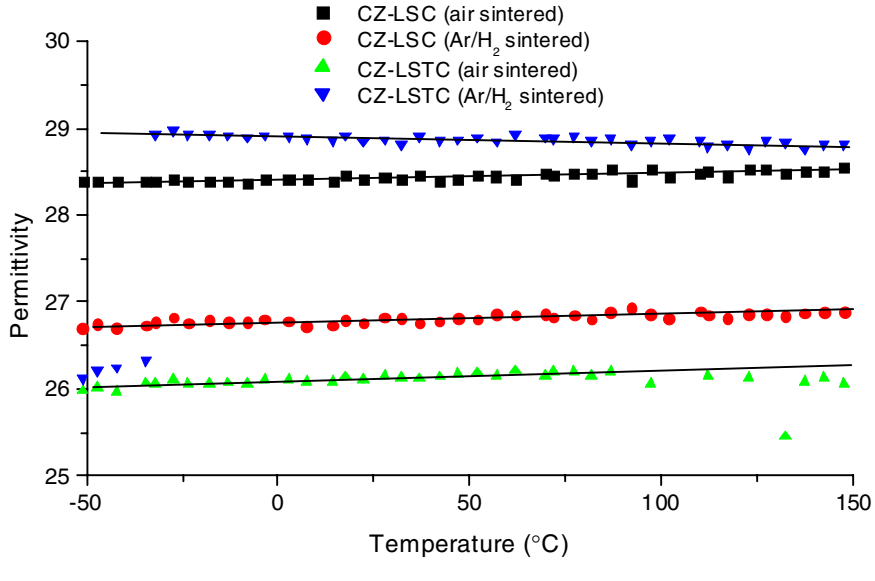

Figure 20 Evolution of the permittivity of the CZ-LS(T)C samples sintered in oxidising or reducing atmosphere.

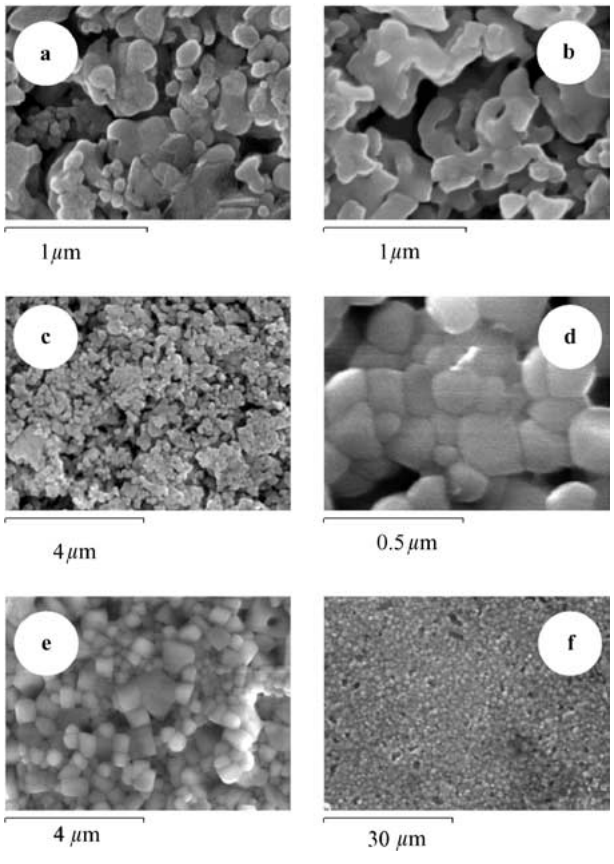

Figure 21 Microstructure of CZ-LSC water-quenched-samples (a: 650°C; b: 750°C; c: 950°C; d: 1000°C; e: 1100°C; f: 1200°C).

modify the doping rate and to try to substitute the A or B site of the perovskite rather than to simply add these elements to the stoichiometric phase, nevertheless it is not the aim of this article and this study is sill opened. Finally, note that B_2O_3-doped sample, i.e., the only one sintered at 1200°C, exhibits attractive properties with $\varepsilon = 31.4$ and dielectric losses less than 0.1% at 1 MHz, an insulating resistivity of 10^{13} Ω·cm, a temperature coefficient of 24 ppm/K and a QF product at 15.9 GHz equal to 34 THz.

Owing to the main aim of this paper, this first part can be summarised in a very few words, remembering that none of the sintering aids was efficient enough to consent to a sintering bellow the copper melting point. Nevertheless, all of these doping agents are sufficient to permit a co-sintering with nickel electrodes. Moreover, it has been shown that the permittivity can be slightly enhanced using certain dopant such as TiO_2 or SiO_2. These numerous prospective tests applied to $CaZrO_3$ also offer an important range of doping agents able to allow a fine control of the temperature coefficient τ_ε.

3.2. A sintering aid addition for low firing temperature

This second part is dedicated to the low temperature sintering of the $CaZrO_3$-based material and to its characterisation. Based upon the above results and those reported in [6], a test combining several alloys was carried out, the objective being to both reduce the sintering temperature and naturally to maintain the good dielectric properties of the material. Four dopants were kept: $LiNO_3$, $CaCO_3$, amorphous SiO_2 and TiO_2. $LiNO_3$ was chosen since it has proved to be efficient to reduce efficiently the sintering temperature. The idea was the same concerning the use of $CaCO_3$. SiO_2 was chosen for two reasons. First, it is well known in SiO_2 glasses that the lithium can promote a low melting temperature and can lower the viscosity of the liquid phase; both these effects could enhance the densification. Secondly, an excess of Ca^{2+} is introduced and this ion was assumed to enter the $CaZrO_3$ structure; consequently, the choice was made to add an ion, Si^{4+}, that could compensate for the induced non-stoichiometry. This last point has also motivated the tests carried out using the TiO_2 doping. Finally, note that these two valence IV cations also offer advantages in terms of dielectric properties: the doped-samples present the two highest permittivities (Fig. 9) among all the compositions reported in the first part and the Ti- and Si-doped samples display opposite temperature coefficients, which can be used to adjust

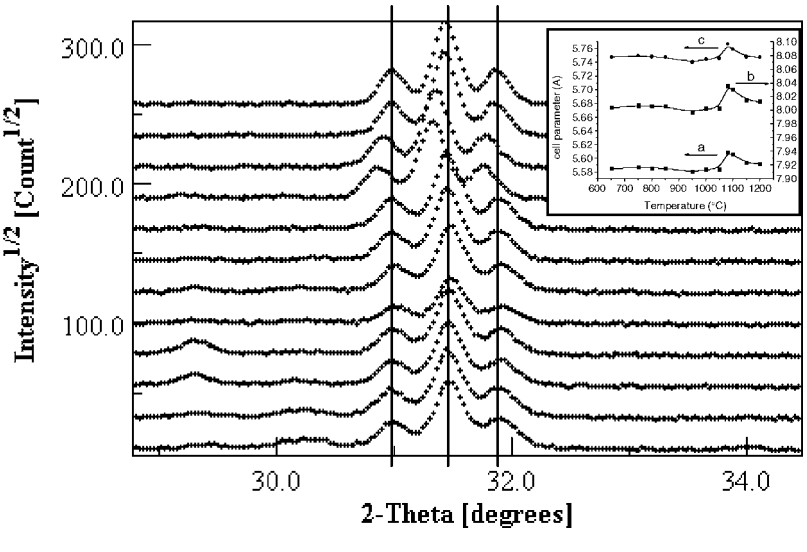

Figure 22 Evolution of the X-ray patterns as a function of the quench temperatures. From bottom to top: 650, 750, 800, 850, 900, 950, 1000, 1050, 1080, 1100, 1150, 1200°C. The inset shows the lattice parameters evolution as a function of the quench temperatures.

TABLE I Additions to $CaZrO_3$ for the experiments plan

L	C	S	LC	LS	CS	LCS	Av.	$\%d$	m_f/m_i	T_{MSR}
−1	−1	−1	1	1	1	−1	1	80%	96%	1500
−1	−1	1	1	−1	−1	1	1	89%	96%	1290
−1	1	−1	−1	1	−1	1	1	81%	96%	1400
−1	1	1	−1	−1	1	−1	1	89%	95%	1345
1	−1	−1	−1	−1	1	1	1	76%	93%	1300
1	−1	1	−1	1	−1	−1	1	91%	95%	1050
1	1	−1	1	−1	−1	−1	1	74%	94%	1240
1	1	1	1	1	1	1	1	90%	93%	1192

TABLE II Results of the experiments plan ($\%d$ in percent, m_f/m_i in percent and T_{SRM} in °C)

	L	C	S	LC	LS	CS	LCS	Av.
$\%d$	−0.9	−0.3	6.0	−0.3	1.9	0.0	0.1	83.7
m_f/m_i	−1.0	−0.4	0.1	−0.1	0.1	−0.4	−0.2	94.7
T_{MSR}	−94.1	4.7	−70.4	15.9	−4.1	44.6	5.9	1290

the one of this multi-alloys-doped material. In a first step, only the $LiNO_3$, $CaCO_3$ and SiO_2 dopant were used. This system was analysed using simply a 2^3 experiments plan (3 parameters and 2 levels used for each parameter) [72, 73]. The levels for the doping agents are (−1) when a specified dopant is not used and (+1) when it is used. When they were used, the amounts of dopant were respectively 5 mol%, 2.5 mol% and 2.5 mol% for $LiNO_3$, $CaCO_3$ and SiO_2. These 3 parameters were simultaneously studied through dilatometric measurements. Table I summarises the different additions to $CaZrO_3$ and the results of the experiments plan are given in Table II. The uncertainty on the relative density being around 2%, the only significant effects can be attributed to the presence of SiO_2 and eventually to the combined action of SiO_2 and $LiNO_3$, which improve the density (after a thermal cycle that reaches 1400°C for the dilatometric measurements). The mass losses are due to the departure of the NO_x of $LiNO_3$ and CO_2 of the calcium carbonate. The most interesting parameter concerns the evolution of T_{SRM} and owing to this simple analysis, some results emerges: (i) the beneficial effect of $LiNO_3$ is confirmed and it is the most interesting in terms of sintering temperature decrease; (ii) the SiO_2-doping displays an as attractive behaviour; (iii) the Ca + Si combination seems to be deleterious for the reducing of the sintering temperature; this could be interpreted in terms of secondary phase formation ($CaSiO_3$), which prohibits the silicon oxide from participating to the sintering temperature decrease; (iv) the Ca + Li combination seems to be slightly detrimental, nevertheless, no explanation is given for this. Additional tests were carried out to optimise the composition. Based on the assumption that the SiO_2 addition needed to be compensated (if it enters the perovskite structure), the $CaCO_3$ addition was kept. Few trials made by increasing the $LiNO_3$ content and/or diminishing the $CaCO_3$ one (and consequently the SiO_2 one too) are represented in Fig. 18. The best result emerging from the experiments plan is also plotted as a comparison ($CaZrO_3$ + 5 mol% $LiNO_3$ + 2.5 mol% amorphous SiO_2). It is shown that simply doubling all the dopants amounts ($CaZrO_3$ + 10 mol% $LiNO_3$ + 5 mol% amorphous SiO_2 + 5 mol% $CaCO_3$) is not sufficient to reduce the sintering temperature, but if, in addition, the amounts of $CaCO_3$ and SiO_2 are decreased (3 mol%), the T_{SRM} is reduced by nearly 100 K. Note that the use of quartz instead of amorphous SiO_2 shifts the sintering temperature to higher temperature by nearly 130 K. In the same plot (Fig. 18), the dilatometric results for two samples with this last composition ($CaZrO_3$ + 10 mol% $LiNO_3$ + 3 mol% amorphous SiO_2 + 3 mol% $CaCO_3$) sintered at 1000°C and 1500°C are displayed. It is evidenced that a sintering at 1000°C is sufficient to obtain an almost full densification. Adding the titanium oxide ($CaZrO_3$ + 10 mol% $LiNO_3$ + 2.5 mol% amorphous SiO_2 + 2.5 mol% TiO_2 + 5 mol% $CaCO_3$), the densification temperature is shifted to higher temperature by about 50 K. This two composition will be referred in the following as CZ-LSC for the first one and CZ-LSTC for the second one. Samples with these compositions were sintered at 1000°C for 6 h with a heating and cooling ramp of 150 K/h. The densities reached are 4.3 for the CZ-LSC samples and 4.2 for the CZ-LSTC samples, whatever the atmosphere (the density of $CaZrO_3$ is 4.62). The microstructure of the air sintered CZ-LSC sample is shown in Fig. 19. This microstructure of a polished surface is representative of the one of all the four samples (CZ-LSC and CZ-LSCT in air or in reducing atmosphere). Their dielectric properties measured at 1 MHz are shown on Fig. 20. Both these compositions exhibit very attractive properties both using an oxidising or reducing atmosphere. In the case of CZ-LSC, the use of a reducing atmosphere decreases the permittivity (from 28.4 to 26.2 at round temperature) and the temperature coefficient τ_ε is roughly maintained (from 26 to 31 ppm/K). Conversely, in the case of CZ-LSTC, the reducing atmosphere contributes to an increase of the permittivity from 26.2 to 28.9 and the temperature coefficient changes in sign from –12 to 43 ppm/K. Note in this last case that the negative temperature coefficient for the samples sintered in air is in agreement with the observed value for the TiO_2-doped sample discussed in the first part (Fig. 9). It is thought that a rigorous control of the atmosphere could allow to maintain τ_ε near zero. The dielectric losses were too low ($<10\times10^{-4}$) to be measured at 1 MHz. These compositions were also made into pellets to measure their dielectric properties at high frequency using the cavity method. The QF products (in THz) are respectively 16.3 (air) and 13.5 (Ar/H_2) for the CZ-LSC sample and 14 (air) and 15.2 (Ar/H_2) for the CZ-LSTC sample. The permittivities are respectively 27.6 (air) and 27.9 (Ar/H_2) for the CZ-LSC sample and 28 (air) and 27.8 (Ar/H_2) for the CZ-LSTC sample. These high frequency measurements evidence a small evolution of the dielectric properties versus the atmosphere used during the sintering. Whereas the change of atmosphere from an oxidising one to a reducing one slightly enhances the QF of the CZ-LSTC sample, it diminishes the QF of the CZ-LSC sample. This behaviour suggests an unnegligible positive contribution of the titanium. This result was surprising since this ion was thought to be partially

reduced from Ti^{4+} to Ti^{3+} during the sintering under reducing atmosphere, promoting the formation of additional charge carriers. No satisfying interpretation has yet been found to explain this unexpected behaviour. The insulating resistivities are all around 10^{12} Ω·cm and owing to the uncertainty on this measurement, no comparison can be made between the different samples. A sample with the CZ-LSC composition was heated and water-quenched at several temperatures (where the densification rate in non-zero, from 650 to 1200°C with a 50°C step) in order to observe the different stages of its densification. Some microstructures are presented in Fig. 21. The first one (Fig. 21a) represents the microstructure at the beginning of the sintering at 650°C. The particles are small ($\leq$ 150 nm) and dispersed; the porosity is very large. In Fig. 21b, one can see the particles coming closer and more or less weak necks forming between them. Fig. 21c shows the microstructure of a sample quenched at 950°C = T_{SRM}; the microstructure appears as heaps of joined particles; the necks are already well defined and some bigger particles begin to absorb the smallest ones. The next microstructure (Fig. 21d) represents the one of a sample quenched at 1000°C; the particles size is comprised between 100 and 250 nm evidencing the growth of the grains and revealing structures characteristic of the intermediate stage of the sintering with evident dihedral angles at the boundary intersection and a continuous pore phase [74, 75]. Fig. 21e represents the 1100°C quenched sample; the grains have a polyhedral shape and their size is greater than 400 nm; no porous channels are visible and there remains only closed porosity. Finally, Fig. 21f represents the 1200°C quenched sample; the particle size is comprised between 600 nm and 1.5 μm; there are still remaining closed pores homogeneously dispersed in the microstructure. None of these microstructures evidence any liquid phase formation and neither do the EDS support this idea (no additional phase between the grains or at the grain surface). Nevertheless, the amount of added flux is sufficiently low to hardly appear on the microstructure; moreover, the lithium ion is not visible through our EDS analysis (Be window). Finally, all these quenched samples were analysed by X-ray diffraction. The results are plotted in Fig. 22. All these patterns were fitted using the software MAUD (Material Analysis Using Diffraction written by Luca Lutterotti). First, note the presence of the small peak at $2\theta = 29.37°$ which belongs to the $CaCO_3$ phase. This peak remains until 950°C and has entirely disappeared at 1000°C. The most surprising feature concerns the $CaZrO_3$ phase with an evolution of the cell parameters as a function of the temperature. This behaviour is plotted in the inset in Fig. 22 and lines are also drawn on the patterns as guides for the eyes. The most spectacular effect is the increase in cell's parameters till 1050°C up to 1150°C. It appears during the grain growth and could be due to the entrance of the lithium ions in the $CaZrO_3$ structure, since it is slightly bigger than the zirconium in the six-fold coordination (0.74 Å). The following decrease (till 1150°C) in the cell's parameters dimensions could hence be explained by the lithium departure of the ceramic, which would agree with the absence of remaining lithium in samples doped with lithium salts [6, 7]. It would be interesting to confirm or invalidate this scheme. A second effect, more discreet, can be observed at around 950°C, which is the T_{SRM}, when the parameters slightly decrease. This effect could be due either to the entrance in the structure of a small ions like Si^{4+} (0.4 Å in six-fold coordination) or more probably, since the most important effect is observed for T_{SRM}, to the loss in the structure of diffusing atoms.

4. Conclusion

Several known sintering aids were tested in a systematic study to try to lower the $CaZrO_3$ ceramic sintering temperature. Among all these additions, a few emerges as interesting aids as the heavier alkali earths or the boron oxide, nevertheless, none of them is sufficient to allow a sintering bellow the melting point of the copper. In parallel, several additions promote the dielectric properties with QF product as high as 47 THz with a WO_3-doping, permittivity enhancement (up to 33), lowering of the temperature coefficient τ_ε and increase of the insulating resistivity. Owing to past works [6, 7] and to the present study, a combination of dopants was tested and optimised, resulting in a low fireable composition based on $CaZrO_3$, $LiNO_3$, SiO_2 and eventually TiO_2. The samples sintered at 1000°C exhibit very attractive properties, with a QF product of nearly 15, $\varepsilon \sim 28$, a near zero τ_ε and $\rho_i \sim 10^{12}$ Ω·cm. These properties are roughly maintained when the samples are sintered in a reducing atmosphere. Although it could not be observed, the sintering process is though to be due to the formation of liquid phase based upon $LiNO_3$ and SiO_2. It was evidenced that the lattice parameters evolves during the sintering, passing through a minimum for the temperature of maximum shrinkage rate and through a maximum during the coarsening stage. The second part of this article will concern the study of the copper co-sintered chips: their feasibility, optimisation and electrical and dielectric properties.

Acknowledgements

The authors wish to thank the TEMEX Society for collaborating with us and allowing us to publish this work.

References

1. D. W. READEY and M. A. RITLAND Processing and Fabrication of Advanced Material IV, edited by T. S. Srivatsan and J. J. Moore (The Minerals, Metals & Materials Society, 1996) p. 151.
2. O. DOMINGUEZ and J. BIGOT, NanoStruct. Mater. **6** (1995) 877.
3. T. R. G. KUTTY, P. V. HEGDEK, K. B. KHAN, U. BASAK, S. N. PILLAI, A. K. SENGUPTA, G. C. JAIN, S. MAJUMDAR, H. S. KAMATH and D. S. C. PURUSHOTHAM, *J. Nucl. Mater.* **305** (2002) 159.
4. Y. HARADA, *J. Nucl. Mater.* **245** (1997) 217.
5. A. POIRSON, P. DECORSE, G. CABOCHE and L. C. DUFOUR, *Solid State Ion.* **99** (1997) 287.
6. M. POLLET, S. MARINEL and G. DESGARDIN, *J. Europ. Ceram. Soci.* in press.
7. M. POLLET and S. MARINEL, *ibid.* **23**(11) (2003) 1925.
8. Introduction to Powder Metallurgy, Chapter 4, p. 200.
9. M. F. YAN, *Mater. Sci. Engng.* **48** (1981) 53.

10. J. KANTERS, U. EISELE, and J. RÖDEL, *Acta Materialia* **48** (2000) 1239.
11. K. DARCOVICH, L. BÉRA and K. SHINAGAWA, *Mater. Sci. and Engng.* A **341** (2003) 247.
12. FUH-SHAN SHIAU, TSANG-TSE FANG and TSUNG-HSING LEU, *Mater. Chem. Phys.* **57** (1998) 33.
13. R. N. LUMLEY and G. B. SHAFFER, *Scripta Materialia* **35**(5) (1996) 589.
14. B. P. BORGLUM and R. C. BUCHANAN, in Proceedings of the 45th Annual Meeting of the Electron Microscopy Society of America, edited by G. W. Bailey (San Francisco Press, 1987).
15. F. KULCSAR, *J. Amer. Ceram. Soc.* **39**(1) (1956) 13.
16. J. S.CHOI and H. G. KIM, *J. Mater. Sci.* **27**(5) (1992) 1285.
17. J. M. HAUSSONNE, G. DESGARDIN, P. BAJOLET and B. RAVEAU, *J. Amer. Ceram. Soc.* **66**(11) (1983) 801.
18. G. DESGARDIN, I. MEY, B. RAVEAU and J. M. HAUSSONNE, *Amer. Ceram. Soc. Bull.* **64**(4) (1985) 564.
19. D. TOLINO and J. BLUM, *J. Amer. Ceram. Soc.—Commun. Amer. Ceram. Soc.* **68**(11) (1985) C292.
20. H. ANDERSON and M. PROUDIAN, 6th International Conference on Sintering, University of Notre-Dame, Paris, 6–8 June 1983.
21. J. M. HAUSSONNE, J. LOSTEC, O. REGRENY, G. DESGARDIN, B. RAVEAU and P. BAJOLET *Silicates Industriels* (1984) 11.
22. K. KLEVELAND, M. A. EINARSRUD and T. GRANDE, *J. Europ. Ceram. Soc.* **20**(2) (2000) 185.
23. L. QIAO, H. ZHOU, K. CHEN and R. FU, *ibid.* in Press.
24. E. EREMINA, A. KRAVCHENKO, P. KAZIN, Y. TRETYAKOV and M. JANSEN, *Superconductor Sci. Techn.* **11** (1998) 223.
25. H. KANAI, O. FURUKAWA, S. I. NAKAMURA and Y. YAMSHITA, *J.Mater. Sci.* **31** (1996) 1609.
26. D. W. KIM, D. G. LEE and K. S. HONG, *Mater. Res. Bull.* **36** (2001) 585.
27. C. L. HUANG and C. S. HSU, *ibid.* **36** (2001) 2677.
28. C. L. HUANG and M. H. WENG, *ibid.* **36** (2001) 2741.
29. C. L. HUANG and K. H. CHIANG, *ibid.* **37** (2002) 1941.
30. T. HU, H. JANTUNEN, A. UUSIMAKI and S. LEPPAVUORI, *Mater. Sci. Semicond. Proc.*, in Press.
31. Z. HE, J. MA, Y. QU and X. FENG, *J. Europ. Ceram. Soc.* **22** (2002) 2143.
32. Y. HAITAO, G. LING, Y. RUNZHANG, Y. GUOTAO and H. PEIYUN, *Mater. Chem. Phys.* **69** (2001) 281.
33. M. MORI, T. YAMAMOTO, T. ICHIKAWA and Y. TAKEDA, *Solid State Ion.* **148** (2002) 93.
34. C. L. HUANG and Y. C. CHEN, *J. Europ. Ceram. Soc.* **23** (2003) 167.
35. C. L. HUANG, M. H. WENG and H. L. CHEN, *Mater. Chem. Phys.* **71** (2001) 17.
36. Y. R. WANG and S. F. WANG, *Intern. J. Inorg. Mater.* **3** (2001) 1189.
37. N. REZLESCU, L. SACHELARIE, E. REZLESCU, C. L. SAVA and P. D. POPA, *Ceram. Intern.* **29**(1) (2003) 107.
38. K. ALBERTSEN, D. HENNINGS and O. STEIGLEMANN, *J. Electroceram.* **2**(3) (1998) 193.
39. P. HANSEN, D. HENNINGS and H. SCHREINEMACHER, *ibid.* **2**(2) (1998) 85.
40. *Idem., J. Amer. Ceram. Soc.* **81**(5) (1998) 1369.
41. W. H. LEE, T. Y. TSENG and D. HENNINGS, *ibid.* **83**(6) (2000) 1402.
42. W. H. LEE, T. Y. TSENG and D. HENNINGS, *J. Mater. Sci. Mater. Electr.* **11** (2000) 157.
43. C. VIGREUX, B. DENEUVE, J. EL FALLAH and J. M. HAUSSONNE, *J. Europ. Ceram. Soc.* **21**(10/11) (2001) 1681.
44. J. A. CERRI, E. R. LEITE, D. GOUVEA, E. LONGO and J. ARANA VARELA, *ibid.* **79**(3) (1996) 799.
45. W. C. LAS, D. GOUVEA and W. SANO, *Solid State Sci.* **1** (1999) 331.
46. C. L. HUANG, M. H. WENG, C. T. LION and C. C. WU, *Mater. Res. Bull.* **35** (2000) 2445.
47. C. G. SHI and I. M LOW, *ibid.* **33**(6) (1998) 817.
48. E. R. NIELSEN, E. RINGGAARD and M. KOSEC, *J. Europ. Ceram. Soc.* **22**(11) (2002) 1847.
49. L. BENZIDA and J. RAVEZ, *J. Fluor. Chem.* **73** (1995) 69.
50. L. BENZIADA-TAÏBI and H. KERMOUN, *ibid.* **96** (1999) 25.
51. M. POLLET and S. MARINEL, *Mater. Sci. Engng.* A, submitted.
52. T. YAMGUSHI, Y. KOMATSU, T. OTOBE and Y. MURAKAMI, *Ferroelectrics* **27** (1980) 273.
53. B. P. BORGLUM and R. C. BUCHANAN, Ceramic Transaction, Vol. I, "Ceramic Powder Science II, A", edited by G. L. Messing *et al.* (American Ceramic Society, Colombus, OH, 1988).
54. M. POLLET, M. DATURI and S. MARINEL, *Mater. Sci. Engng.* B, In press.
55. Y. SUZUKI, P. E. D. MORGAN and T. OHJI, *J. Amer. Ceram. Soc.* **83**(8) (2000) 2091.
56. K. CVETKOVIC and A. PETRIC, *Amer. Ceram. Soc. Bull.* **79** (2000) 65.
57. J. H. CHOY, Y. S. HAN, S. H. HWANG, S. H. BYEON and G. DEMAZEAU, *J. Amer. Ceram. Soc.* **81**(12) (1998) 3197.
58. J. A. BADENES, M. LLUSAR, J. CALBO, M. A. TENA and G. MONROS, *British Ceram. Trans.* **101**(4) (2002) 158.
59. B. B. KARKI, R. M. WENTZCOVITCH, S. DE GIRONCOLI and S. BARONI, *Phys. Rev.* B **62**(22) 14750.
60. S. JANASWAMY, E. D. DIAS and G. SREENIVASA MURTHY, *Bull. Mater. Sci.* **20**(1) (1997) 23.
61. S. JANASWAMY, G. SREENIVASA MURTHY, E. D. DIAS and V. R. K. MURTHY, *Mater. Lett.* **55** (2002) 414.
62. K. FUKUDA and R. KITOH, *J. Amer. Ceram. Soc.* **77**(1) (1994) 149.
63. B. A. WECHSLER and R. B. VON DREELE, *Acta. Crystallogr.* B **45** (1989) 542.
64. G. R. FISCHER, L. J. MANFREDO, R. N. MCNALLY and R. C. DOMAN, *J. Mater. Sci.* **16**(12) (1981) 3447.
65. A. K. CHATERJEE and G. I. ZHMOIDIN, *ibid.* **7**(1) (1972) 93.
66. G. ROULT, R. PASTUSZAK, R. MARCHAND and Y. LAURENT, *Acta Crystallogr.* **C39** (1983) 673.
67. R. D. SHANNON, *ibid.* A **32** (1976) 751.
68. J. GARCIA-JACA, J. L. MESA, M. INSAUSTI and J. I. R. LARRAMENDI, *Mater. Res. Bull.* **34**(2) (1999) 289.
69. A. W. SLEIGHT, *Acta Crystallogr.* **B28** (1972) 2899.
70. M. MORINAGA, J. B. COHEN and J. FABER, JR, *ibid.* A **35** (1979) 789.
71. P. DURAN, P. RECIO and J. M. RODRIGUEZ, *J. Mater. Sci.* **22** (1987) 4348.
72. J. GOUPY, "Methods for Experimental Design. Principles and Applications for Physicists and Chemists" (Elsevier, Amsterdam 1993).
73. G. SADO and M. C. SADO, AFNOR Technique (1991).
74. R. L. COBLE, *J. Appl. Phys.* **32**(5) (1961) 787.
75. R. L. COBLE, *ibid.* **36**(2) (1965) 2327.

Received 10 June
and accepted 13 November 2003